REPORT DOCUMENTATION PAGE

Form Approved
OMB No. 0704-0188

1. REPORT DATE *(DD-MM-YYYY)*	2. REPORT TYPE	3. DATES COVERED *(From - To)*
12-09-2003	Technical Paper	

4. TITLE AND SUBTITLE

Quantum and Classical Studies of the $O(^3P) + H_2(v=0\text{-}3,j=0) \rightarrow OH + H$ Reaction Using Benchmark Potential Surfaces

5a. CONTRACT NUMBER
F04611-03-C-0015

5b. GRANT NUMBER

5c. PROGRAM ELEMENT NUMBER

6. AUTHOR(S)

M. Braunstein and S. Adler-Golden (Spectral Sciences, Inc.); B. Maiti and G.C. Schatz (Northwestern Univ.)

5d. PROJECT NUMBER
BMSB

5e. TASK NUMBER
R2FT

5f. WORK UNIT NUMBER

7. PERFORMING ORGANIZATION NAME(S) AND ADDRESS(ES)

Spectral Sciences Incorporated
99 South Bedford Street, #7
Burlington MA 01803-5169

8. PERFORMING ORGANIZATION REPORT NUMBER

9. SPONSORING / MONITORING AGENCY NAME(S) AND ADDRESS(ES)

Air Force Research Laboratory (AFMC)
AFRL/PRS
5 Pollux Drive
Edwards AFB CA 93524-7048

10. SPONSOR/MONITOR'S ACRONYM(S)

11. SPONSOR/MONITOR'S NUMBER(S)
AFRL-PR-ED-TP-2003-229

12. DISTRIBUTION / AVAILABILITY STATEMENT

Approved for public release; distribution unlimited.

13. SUPPLEMENTARY NOTES

For presentation in the Journal of Chemical Physics.

14. ABSTRACT

15. SUBJECT TERMS

16. SECURITY CLASSIFICATION OF:			17. LIMITATION OF ABSTRACT	18. NUMBER OF PAGES	19a. NAME OF RESPONSIBLE PERSON
					Leilani Richardson
a. REPORT	b. ABSTRACT	c. THIS PAGE	A	22	19b. TELEPHONE NUMBER *(include area code)*
Unclassified	**Unclassified**	**Unclassified**			(661) 275-5015

Quantum and Classical Studies of the $O(^3P) + H_2(v=0\text{-}3,j=0) \rightarrow OH + H$ Reaction Using Benchmark Potential Surfaces

M. Braunstein* and S. Adler-Golden

Spectral Sciences, Incorporated, Burlington, Massachusetts 01803

(*Electronic mail: matt@spectral.com)

B. Maiti and G. C. Schatz

Department of Chemistry, Northwestern University, Evanston, Illinois 60208-3113

Abstract

We present results of time dependent quantum mechanics (TDQM) and quasi-classical trajectory (QCT) studies of the excitation function for $O(^3P) + H_2(v=0\text{-}3,j=0) \rightarrow OH + H$ from threshold to 30 kcal/mol collision energy using benchmark potential energy surfaces [Rogers *et al.* J. Phys. Chem. A **104**, 2308 (2000)]. For $H_2(v=0)$ there is excellent agreement between quantum and classical results. The TDQM results show that the reactive threshold drops from 10 kcal/mol for v=0 to 6 for v=1, 5 for v=2 and 4 for v=3, suggesting a much slower increase in rate constant with vibrational excitation above v=1 than below. For $H_2(v>0)$, the classical results are larger than the quantum results by a factor ~2 near threshold, but the agreement monotonically improves until they are within ~10% near 30 kcal/mol collision energy. We believe these differences arise from stronger vibrational adiabaticity in the quantum dynamics, an effect examined before for this system at lower energies. We have also computed QCT OH(v,'j') state-resolved cross sections and angular distributions. The QCT state-resolved OH(v') cross sections peak at the same vibrational quantum number as the H_2 reagent. The OH rotational distributions are also quite 'hot' and tend to cluster around high rotational quantum numbers. However, the dynamics seem to dictate a cutoff in the energy going into OH rotation. The state-resolved OH distributions were fit to probability functions based on conventional information theory extended to include an 'energy gap' law for product vibrations and angular momentum constraints for product rotations.

Quantum and Classical Studies of the $O(^3P) + H_2(v=0\text{-}3,j=0) \rightarrow OH + H$ Reaction Using Benchmark Potential Surfaces

M. Braunstein* and S. Adler-Golden

Spectral Sciences, Incorporated, Burlington, Massachusetts 01803

(*Electronic mail: matt@spectral.com)

B. Maiti and G. C. Schatz

Department of Chemistry, Northwestern University, Evanston, Illinois 60208-3113

Abstract

We present results of time dependent quantum mechanics (TDQM) and quasi-classical trajectory (QCT) studies of the excitation function for $O(^3P) + H_2(v=0\text{-}3,j=0) \rightarrow OH + H$ from threshold to 30 kcal/mol collision energy using benchmark potential energy surfaces [Rogers *et al.* J. Phys. Chem. A **104**, 2308 (2000)]. For $H_2(v=0)$ there is excellent agreement between quantum and classical results. The TDQM results show that the reactive threshold drops from 10 kcal/mol for v=0 to 6 for v=1, 5 for v=2 and 4 for v=3, suggesting a much slower increase in rate constant with vibrational excitation above v=1 than below. For $H_2(v>0)$, the classical results are larger than the quantum results by a factor ~2 near threshold, but the agreement monotonically improves until they are within ~10% near 30 kcal/mol collision energy. We believe these differences arise from stronger vibrational adiabaticity in the quantum dynamics, an effect examined before for this system at lower energies. We have also computed QCT OH(v,'j') state-resolved cross sections and angular distributions. The QCT state-resolved OH(v') cross sections peak at the same vibrational quantum number as the H_2 reagent. The OH rotational distributions are also quite 'hot' and tend to cluster around high rotational quantum numbers. However, the dynamics seem to dictate a cutoff in the energy going into OH rotation. The state-resolved OH distributions were fit to probability functions based on conventional information theory extended to include an 'energy gap' law for product vibrations and angular momentum constraints for product rotations.

I. INTRODUCTION

Recently, the energy-dependent cross section (excitation function) for the reaction $O(^3P)$ + $H_2(v=0) \rightarrow OH + H$ was measured by molecular beam methods and was studied with high-level quantum dynamics[1] using 'benchmark' potential surfaces.[2] Agreement was excellent over a large energy range. The above reaction is of fundamental interest: it is one of the simplest hydrogen abstraction reactions, it is important in many combustion processes, and it is small enough for quantitative theoretical treatments. It has been studied theoretically with quantum[3-9] and classical[10-12] methods on a number of potential surfaces and studied experimentally through measurement of the rate constant.[13] The high barrier to reaction (~13 kcal/mol), however, requires high reagent velocities, and this has made the measurement of the excitation function and state-to-state processes difficult. The increasing capabilities of hyper-velocity O-atom sources, as were used to study the excitation function,[1] should enable the accurate measurement of state-to-state quantities for this 'prototype' reaction in the near future.

In this paper we present results of time dependent quantum mechanics (TDQM) and quasi-classical trajectory (QCT) studies of the excitation function for $O(^3P) + H_2(v,j=0) \rightarrow OH + H$, where the H_2 vibrational quantum number v varies from 0-3, from threshold to 30 kcal/mol collision energy, using the same benchmark potential energy surfaces. Because the vibrational spacings are large, quantum effects should be especially important. Comparison of the results will provide insight into the validity of classical approaches for such a 'worst case.' In addition, the present results will enable us to determine the change in reactivity with increasing excitation of the reactants, which is a subject of interest to fundamental studies of reaction dynamics.[14] In past studies of $O + H_2(v=1)$, it was found that the rate constant is three orders of magnitude larger than for $O + H_2(v=0)$ at room temperature.[15] This implies a reduction in threshold energy from the ~10 kcal/mol value observed for v=0 in the molecular beam measurements to about 6 kcal/mol for v=1. If this trend were to continue, then the threshold could drop to zero for v=3. Large drops in threshold energy have been found before, such as for the $H + H_2O$ reaction.[14] However, the drop in threshold energy with increasing vibrational excitation is very sensitive to the shape of the potential surface, so it is not clear what behavior is to be expected for $O + H_2$. Since high quality surfaces are available for $O + H_2$, we can use this reaction as a benchmark for studying the drop in threshold with increasing vibrational excitation.

An additional component of the present paper is that we have computed QCT OH(v',j') state-resolved cross sections and angular distributions. We show that these OH(v',j') distributions can be fit to probability functions based on conventional information theory[16,17] extended to include an 'energy gap' law[18] for OH vibrations and angular momentum constraints[19,20] for rotations. We compare all our results to experimental data where available and to previous theoretical calculations. These distributions will likely be measured in future reaction dynamics experiments, so our results will be useful for interpreting these measurements.

The O + H_2 (v≥0) reaction is also of interest at high velocities in order to characterize the ambient environment of spacecraft under low earth orbit (LEO) conditions.[21] Spacecraft in low earth orbit continually emit gases due to outgassing, venting, and engine firings. These gases can then interact with the atmosphere, mostly oxygen atoms, at high relative velocities usually near ~8 km/s. The resulting highly excited products, OH(v',j') in the present case, can produce radiative emissions near the vehicle that provide *in-situ* monitoring of the spacecraft environment.

The paper proceeds as follows. In Section II we describe our computational methods. In Section III we present the detailed results, first focusing on the excitation functions, then the state-resolved product distributions, and finally the fits of the distributions. Section IV presents a summary.

II. COMPUTATIONAL METHODS

Scattering calculations were done on the ^{3}A' and ^{3}A'' surfaces of Rogers et al.[2] These surfaces have been used previously to study the O + H_2(v=0,j=0) excitation function with good agreement with measurements.[1] The surfaces were generated from *ab-initio* configuration interaction calculations with a very large basis set, and they are likely the most accurate surfaces to date. Coupling between the two surfaces has been ignored, and the 2^3A'' state which leads to electronically excited products has not been included. From previous studies, these approximations should be of small importance.[5] Likewise, any coupling to singlet surfaces is ignored.

Results were generated using 3D time-dependent quantum mechanics (TDQM) and quasi-classical trajectory (QCT) methods. The TDQM wave packet formalism has been described

previously,[22] including details of the spatial grid and time propagation. To reduce the computational burden, it has been implemented with the centrifugal sudden approximation (CSA), which should be a small approximation based on previous studies of similar systems. For the QCT calculations, we use standard Monte Carlo techniques.[23] The required derivatives of the potentials were computed with a fifth order finite difference method. At least 25,000 trajectories per collision energy per electronic state per initial H_2 vibrational state were generated. For H_2(v=0), a fixed time step of 0.5 a.u. and a maximum impact parameter of 3.0 were used. For H_2(v=1,2) the same time step was used, but the maximum impact parameter was 5.0 a.u. For H_2(v=3) a time step of 0.25 a.u. and maximum impact parameter of 7.0 a.u. were used.

III. RESULTS

A. Total cross sections

The total cross sections for the reaction $O(^3P) + H_2(v,j=0) \rightarrow OH + H$ are shown in Figure 1. The present results are obtained by forming the statistical average of the cross sections for the two separate electronic states considered, (1/3) ($^3A' + {}^3A''$). For H_2(v=0) as seen in a previous study,[1] there is excellent agreement between the TDQM, QCT, and experimental results, except at collision energies near threshold. Although the QM results of Ref. 3 use the same set of potential energy surfaces as the present study, they begin to diverge away from the present results at collision energies of 15 kcal/mol. They are about twice those of the present results at ~23 kcal/mol. It is possible that these differences come from the 'J-shifting' approximation used in Ref. 3 to obtain the $J_{tot} > 0$ cross sections. The QCT results of Ref. 12 agree very well with the present QCT results at energies up to ~25 kcal/mol collision energy. For the H_2(v>0) cross sections we shall see that close agreement up to a certain collision energy is also the case, and this may indicate that the parts of the potential energy surface of Ref. 12 accessed at lower energies may have the same accuracy as the ones used here. The QCT results of Ref. 11 are consistently too large, and this is probably due to inaccuracies of the potential energy surface used in this study near the barrier region.

Examining the TDQM cross sections we see that the reactive threshold energy drops from ~10 kcal/mol for v=0 to 6 kcal/mol for v=1, 5 for v=2 and 4 for v=3. The v=0 to v=1 drop is consistent with what would be expected based on the measured ratio of v=1/v=0 rate constants,[15]

as mentioned in the Introduction. In addition, this change is consistent with expectations discussed for other *ab initio* surfaces[8] that there is a change in the location of the reactive bottleneck from close to the saddle point for v=0 to the reagent side of the saddle point for v=1. For v=2 and 3 we see that the drop in threshold is much smaller than that from v=0 to v=1, indicating only a modest shift in bottleneck location with reagent vibrational excitation. In addition, the threshold remains finite for v=3, even though there is plenty of energy to surmount the barrier.

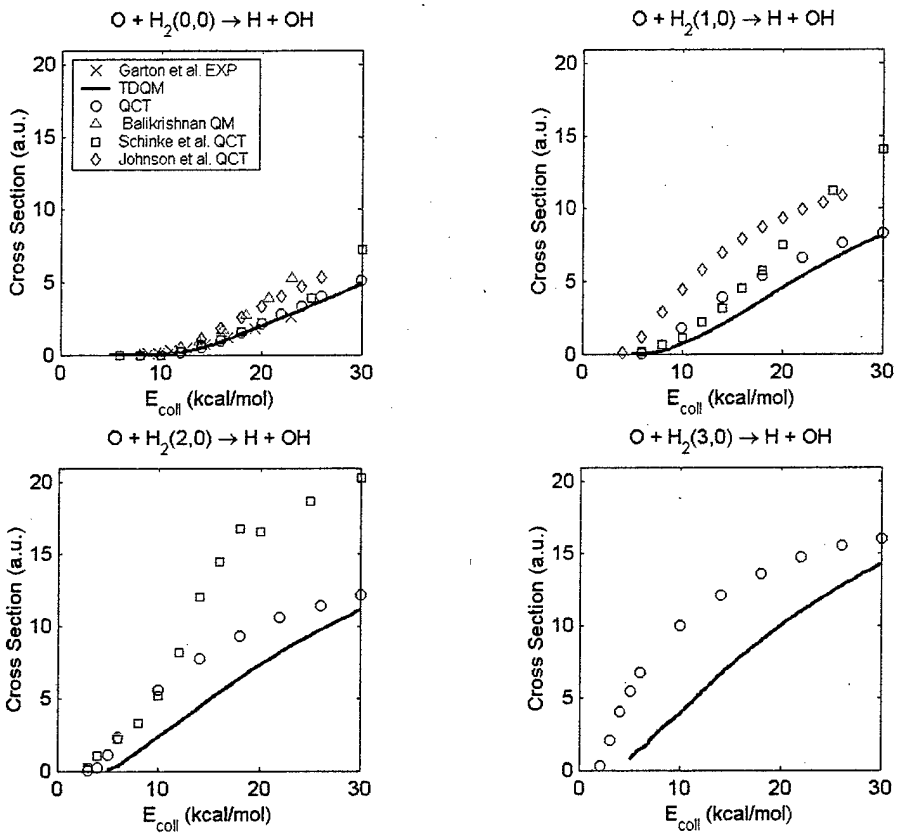

FIG. 1. Total cross sections for $O(^3P) + H_2(v,j=0) \rightarrow OH + H$. Crosses are the experimental results of Ref. 1, solid lines are the present TDQM results, circles are the present QCT results, triangles are the quantum scattering results of Ref. 3, squares are the QCT results of Ref. 12, and diamonds are the QCT results of Ref. 11.

For v>0, present quantum and classical results are now only within a factor of ~2 near threshold (much greater very near threshold) with the QCT results always too large. As the H_2

vibration increases the agreement becomes worse. The agreement monotonically improves with collision energy until the QCT and TDQM cross sections are within ~10% of each near 30 kcal/mol collision energy.

Figure 2 shows the present TDQM and QCT results for $O(^3P) + H_2(v,j=0) \rightarrow OH + H$, but broken down into contributions from each surface. As seen for the total cross sections, the agreement is very good for $H_2(v=0)$, but the QCT results are too high for $H_2(v>0)$ with closer agreement as the collision energy increases.

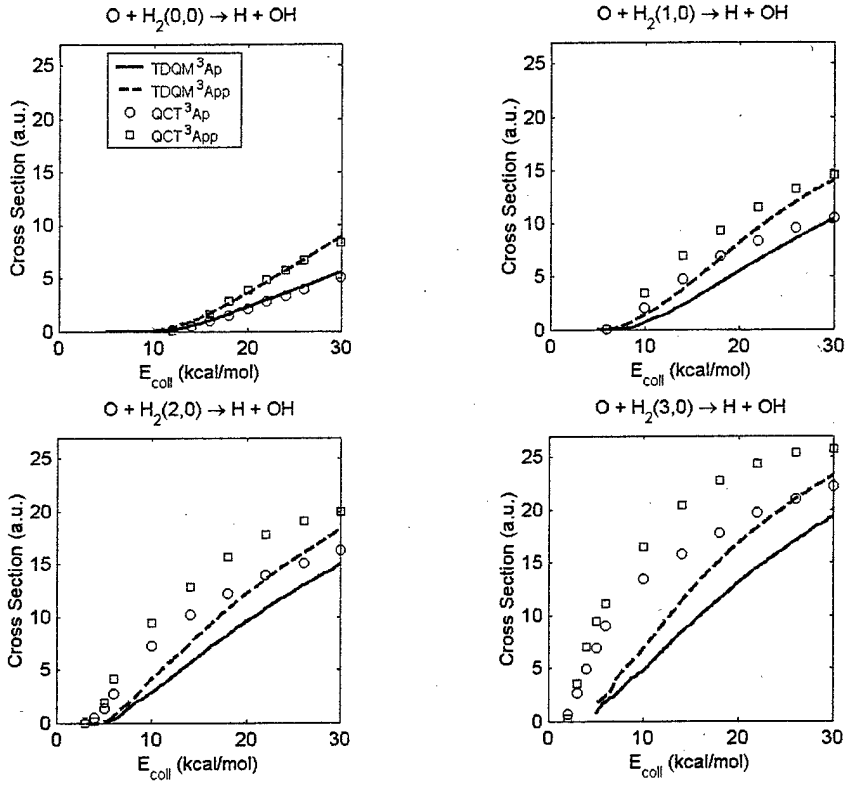

FIG. 2. Cross sections from each electronic surface for $O(^3P) + H_2(v,j=0) \rightarrow OH + H$. Solid lines are for the TDQM results using the $^3A'$ surface, broken lines are for the TDQM results using the $^3A''$ surface, circles are for the QCT results using the $^3A'$ surface, and squares are for the QCT results using the $^3A''$ surface.

We believe the differences between the present TDQM and QCT cross sections arise from differences in vibrational adiabaticity between quantum and classical mechanics (with the quantum results being much more adiabatic), an effect that has been examined before for this system[4,8] (and others[24]) at energies near threshold. As the collision complex is formed, bound

motions perpendicular to the minimum energy reaction path can be defined. The quantized energy associated with these bound motions added to the minimum energy path create effective energy thresholds for reaction. If the reaction is vibrationally adiabatic, it proceeds along the reaction path with constant internal vibrational energy, and it becomes sensitive to these effective energy thresholds. As has been pointed out,[24] due to the uncertainty principle these thresholds can be important even when the time scale for the bound vibration is long compared to the time of the reaction. The neglect of the quantized bound motion along the reaction path in the QCT calculation can therefore make for smaller barrier heights than a quantum approach. This could result in higher QCT cross sections, which is presumably reflected in the present results. As the collision energy becomes much larger than the barrier heights, these effects should diminish, which is what we observe. For H_2(v=0), the barrier location is close to the saddle point in the potential energy surface. But for H_2(v>0), the effective barriers form in the entrance and exit channels, with the entrance channel bottleneck expected to be more significant.[8] This may be important in understanding the difference between classical and quantum results with increasing vibrational quantum number. The QCT calculations also neglect other potentially significant quantum effects such as tunneling, important close to threshold.

A number of procedures have been formulated to correct for vibrational adiabaticity in QCT calculations.[8,24] A simple approach is to adjust the initial vibrational quantum number of the H_2 to better reflect the difference between the collision energy and the true effective barrier heights. We test this idea in Figure 3, where we show the ^{3}A'' TDQM results for v=2 and the corresponding QCT results for v=1, 1.5, 1.75 and 2. Results for an initial quantum number of 1.5 show very

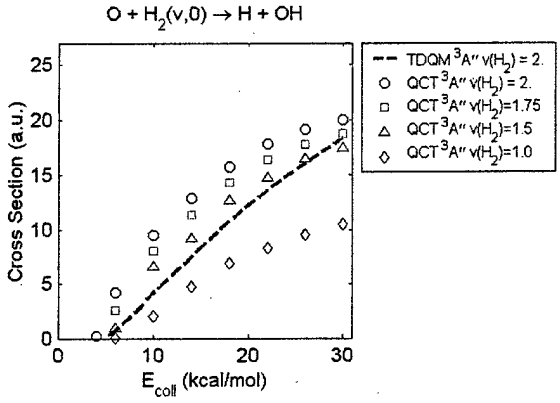

FIG. 3. Comparison of TDQM and QCT cross sections for the ^{3}A'' surface alone. Dashed line is for TDQM with an H_2 quantum number of 2, circles are for QCT with an H_2 quantum number of 2, squares are for QCT with an H_2 quantum number of 1.75, triangles are for QCT with an H_2 quantum number of 1.5, and diamonds are for QCT with an H_2 quantum number of 1.0

good agreement with the TDQM results for most of the energy range. However, we note that the OH product distributions are also affected, and these show an energy cutoff which prevents the higher (v',j') states from being produced, an artifact of this simple procedure.

B. State-resolved cross sections

Figure 4 shows QCT cross sections at 18 kcal/mol collision energy for the reaction $O(^3P)$ + $H_2(v=0\text{-}3,j=0) \rightarrow OH(v') + H$, as a function of initial H_2 vibration and final OH vibration. Results at other collision energies are similar. The results show OH vibrational distributions centered on the same quantum number as the initial H_2 quantum number. This makes for non-thermal product distributions in which a great deal of energy goes into vibration. (Below we fit these distributions using an energy gap law that depends on the difference between the initial and final vibrational energies.) We also show results of QCT calculations of Ref. 12 at 20 kcal/mol collision energy for $H_2(v=0\text{-}2,j=1)$ where we have multiplied their reported probabilities by our total cross sections in order normalize out differences in the overall reaction cross section. The difference between the two QCT calculations for $H_2(v=0)$ and $H_2(v=2)$ and j=1 are so close as to be indistinguishable on this scale. The two QCT results for $H_2(v=1)$ are almost as close. Although at this collision energy the $H_2(v=2)$ total cross sections differ by about a factor of ~2, the vibrational distributions for all initial states seem insensitive to any differences in the potential surfaces of the two QCT calculations. We also note that Broida and Persky[10] have performed similar QCT calculations on LEPS surfaces derived from Ref. 11 for $O + H_2(v=0\text{-}7) \rightarrow OH + H$. Like the present results, they found a significant increase in reactivity with H_2 vibrational

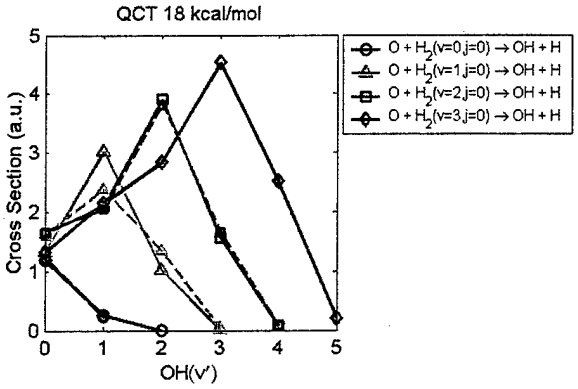

FIG. 4. QCT cross sections for $O(^3P)$ + $H_2(v=0\text{-}3,j=0) \rightarrow OH(v') + H$. Circles are for $H_2(v=0)$, triangles are for $H_2(v=1)$, squares are for $H_2(v=2)$, and diamonds are for $H_2(v=3)$. Solid lines are for the present QCT results at 18 kcal/mol collision energy, while dashed lines are renormalized QCT results of Ref. 12 at 20 kcal/mol collision energy for $H_2(v=0\text{-}2,j=1)$.

excitation and an efficient conversion of vibrational energy from reagents to products (see especially Figure 10 of Ref. 10). We have examined several trajectories from our QCT calculations to understand the origin of these behaviors. Most of the reactive trajectories are 'direct,' with the oxygen atom leaving with the hydrogen it first encounters and the reaction taking place in a vibrational period or less. A quantitative analysis of these trajectories, however, will be required to understand the mechanism behind the observed dynamical behavior. To summarize our QCT results, Table 1 gives the vibrationally resolved cross sections at collision energies of 10, 18, and 26 kcal/mol and the total cross sections for each initial $H_2(v,j=0)$ state. Statistical uncertainties in the QCT calculations give roughly three significant figures for the overall reactive cross section from a given initial H_2 vibrational state, roughly two significant figures for the vibrationally resolved cross sections, and roughly one significant figure for the rotationally resolved cross sections presented below.

E_{coll}=10 kcal/mol	v=0	1	2	3
v' = 0	0.00	0.38	0.75	0.69
1	0.00	1.18	1.39	1.29
2	0.00	0.26	2.74	2.59
3	0.00	0.00	0.72	3.94
4	0.00	0.00	0.00	1.49
Σv' QCT	0.000	1.813	5.605	10.004
Σv' TDQM	0.021	0.676	2.354	3.895

E_{coll}=18 kcal/mol	v=0	1	2	3
v'=0	1.20	1.33	1.65	1.32
1	0.27	3.03	2.11	2.15
2	0.00	1.03	3.92	2.85
3	0.00	0.02	1.58	4.53
4	0.00	0.00	0.08	2.51
5	0.00	0.00	0.00	0.20
Σv' QCT	1.465	5.410	9.34	13.559
Σv' TDQM	1.402	3.678	6.362	8.906

E_{coll}=26 kcal/mol	v=0	1	2	3
v'=0	2.69	1.92	1.92	1.69
1	0.82	3.94	2.58	2.49
2	0.06	1.60	4.24	3.45
3	0.00	0.16	2.36	4.49
4	0.00	0.00	0.31	2.69
5	0.00	0.00	0.02	0.64
6	0.00	0.00	0.00	0.08
Σv' QCT	3.560	7.613	11.428	15.529
Σv' TDQM	3.668	6.850	9.709	12.723

Table 1. QCT vibrationally resolved cross sections (summed over j') in a.u. for $O(^3P)$ + H_2(v,j=0) → OH(v') + H. The bottom of each column shows the sum of the v' cross sections as well as the TDQM results summed over v'.

In Figure 5 we show QCT results for the rotationally resolved cross sections for $O(^3P)$ + H_2(v=0-3,j=0) → OH(v',j') + H at 18 kcal/mol collision energy. As the initial H_2(v) quantum number increases and more energy becomes available to products, the OH rotational distributions peak at higher rotational quantum number, and for v'=3 they correspond to Boltzmann temperatures of ~10-20,000 K. For H_2(v=0) and OH(v'=0), these results are consistent with previous quantum studies (see Table V of Ref. 5) done at lower energies with different potential surfaces. As the final vibrational quantum state of the OH increases and less

energy is available to rotation, an energy cutoff becomes apparent. This is most evident for $O(^3P) + H_2(v=3,j=0) \rightarrow OH(v'=1\text{-}3,j') + H$, where the highest 10-15 available rotational states have a negligible probability. In the next section, we fit these rotationally resolved probability distributions with a functional form taking into account the observed energy cutoff.

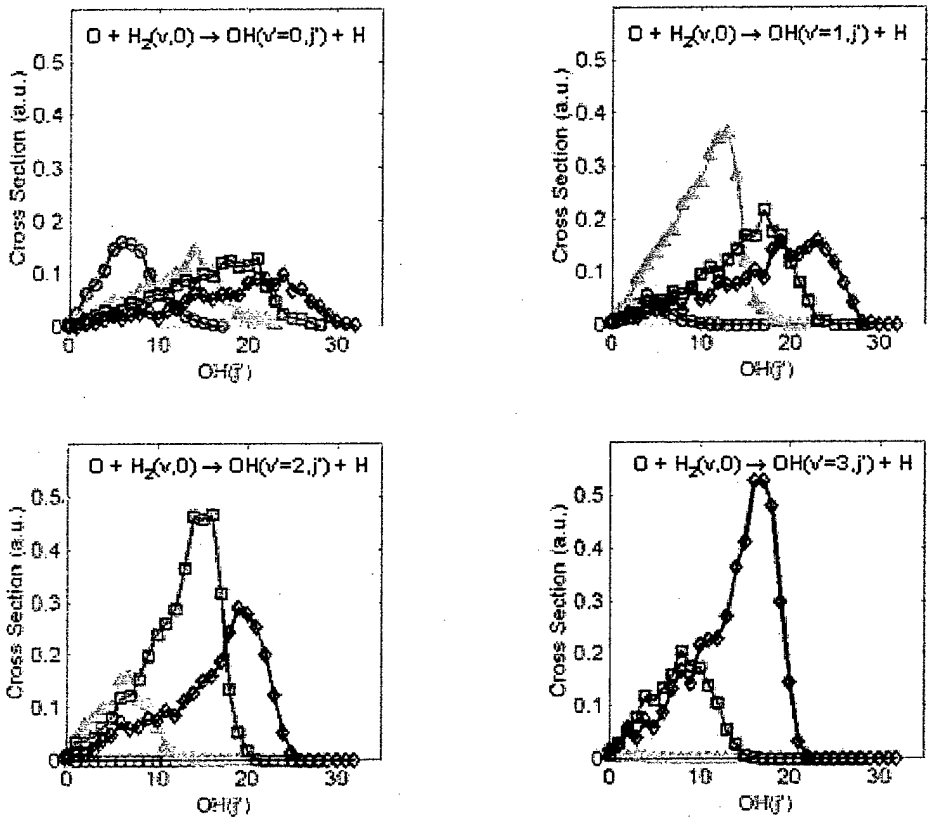

FIG. 5. QCT rotationally resolved cross sections for $O(^3P) + H_2(v=0\text{-}3,j=0) \rightarrow OH(v',j') + H$ at 18 kcal/mol collision energy, showing v'=0 (upper left), 1 (upper right), 2 (lower left) and 3 (lower right). Circles are for $H_2(v=0)$, triangles are for $H_2(v=1)$, squares are for $H_2(v=2)$, and diamonds are for $H_2(v=3)$.

Figure 6 shows the QCT angle resolved differential cross sections in the center of mass frame for $O(^3P) + H_2(v=0\text{-}3,j=0) \rightarrow OH + H$. These cross sections are defined such that:

$$\frac{d\sigma}{d\omega} = \pi b_{\max}^2 \frac{N_r(E_{coll}, v, j=0, \theta)}{N(E, v, j=0)} \frac{1}{4\pi(\sin\theta)\Delta\theta}, \quad (1)$$

where $N_r(E, v, j = 0, \theta)$ is the number of reactive collisions between θ and $\theta + \Delta\theta$. As the H_2(v) quantum number increases, more forward (near 0 degrees) scattering is observed. This has been noted before[12] and ascribed to the increasing importance of the higher impact parameters as the vibrational quantum number increases. Note that for v=3, there is a strong forward peak, indicating that some fraction of the collisions at 18 kcal/mol involve a stripping mechanism.

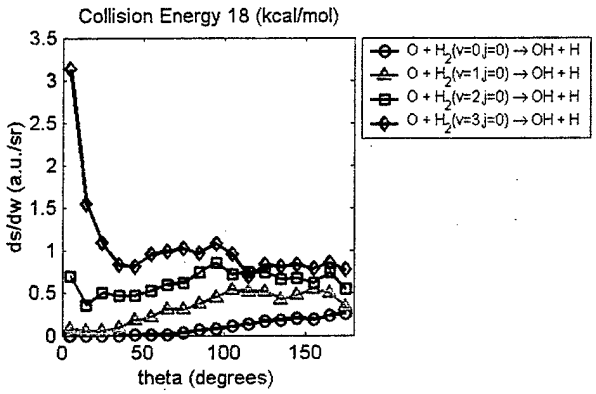

FIG. 6. QCT angle resolved differential cross sections, dσ/dω (a.u./sr), in the center of mass frame for $O(^3P)$ + H_2(v=0-3,j=0) → OH + H. Circles are for H_2(v=0), triangles are for H_2(v=1), squares are for H_2(v=2), and diamonds are for H_2(v=3).

C. Fits of the state-resolved distributions

To further understand the reaction dynamics and facilitate the use of the H + OH product state distributions in kinetics modeling, we fit the distributions to simple functional forms derived from information theory.[16,17] The distributions are given in terms of final state probabilities, P; *i.e.*, ratios of the final state-resolved cross sections to the total reaction cross section for a given collision energy and initial H_2 (v,j) state. In information theory, probabilities are expressed in terms of a prior (statistical) distribution P_0 and a surprisal function, S:

$$P = P_0 \exp(-S). \quad (2)$$

Simple formulas for P_0 are given in the literature.[16,17] For vibrationally resolved distributions, a simple approximation gives $P_0 \propto (E\text{-}E_{v'})^{3/2}$, where E is the energy available to products and $E_{v'}$ is the product internal vibrational energy. S is typically parameterized with a short (e.g., linear) expansion in dynamical variables such as the vibrational or rotational quantum number, vibrational or rotational energy, or energy between initial and final states.

C.1. OH vibrational state distributions

Figure 7 shows surprisal plots (lines with symbols) for the OH(v') state distributions at various collision energies with H_2(v=1,3,j=0). The surprisal is defined -ln(P/P_0), and it gives a measure of deviation away from purely statistical product distributions. A negative surprisal, for example, implies more energy in the products than statistical considerations give alone. The "V" shapes of the plots result from the tendency of the reaction to conserve vibrational energy; that is, for the reaction probability to peak where the OH vibrational energy $E_{v'}$ equals the H_2 vibrational energy E_v. This suggests a parameterization of S involving the vibrational energy gap $|E_{v'} - E_v|$. In addition, a linear surprisal parameter is needed to model the low collision energy cases. Thus, the functional form used to model the vibrational surprisal is

$$S_{v'} = \lambda_v G_{v'} + \lambda_g |E_{v'} - E_v| + C, \quad (3)$$

where $G_{v'}$ is OH vibration energy relative to the total product energy, ($E_{v'}/E$). The λ's are fitting parameters, fit separately for each initial H_2(v) state, and the constant C is set by the requirement that the probabilities over all products for a given initial condition sum to unity. All internal energies are computed from the spectroscopic constants of Ref. 25 that are nearly identical to those derived from the potential surfaces used.

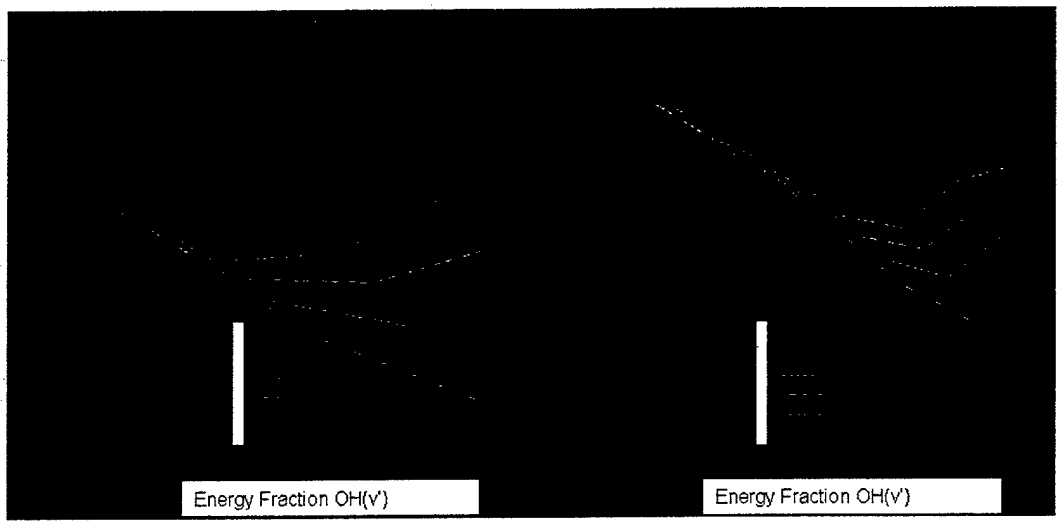

FIG. 7. Vibrational surprisals (lines with symbols) and Eq. 3 fits (symbols only) for O + H_2 (v=1,3) → OH(v') + H as a function of the energy fraction in OH vibration, $G_{v'} = (E_{v'}/E)$.

The surprisal parameters in Eq. (3) were determined from linear least-squares fits to the S_v' for a given E_{coll} and v. When λ_v and λ_g are retrieved simultaneously, they vary somewhat erratically with E_{coll} and v. However, when an average λ_g value of 0.11 per kcal/mol is taken, the retrieved λ_v's behave smoothly as shown in Figure 8, and the model fit S_v's (as shown in Figure 7) still represent the data well. The dependence of λ_v on E_{coll} is approximately exponential and the dependence on E_v is approximately inverse-square-root. As is commonly the case, the vibrational distributions become close to statistical (λ_v close to zero) at high E_{coll}. We also note that the slopes of λ_v as a function of collision energy tend to zero with increasing H_2 vibration.

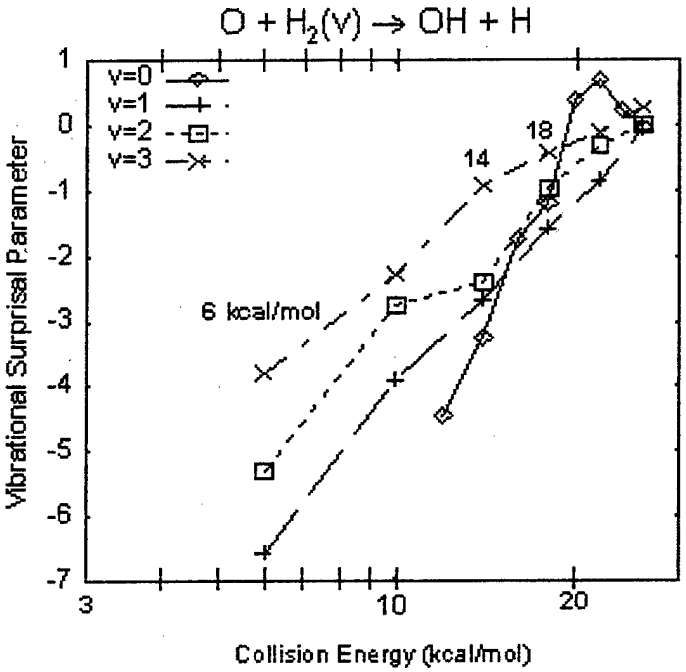

FIG. 8. Dependence of λ_v, the vibrational surprisal parameter, on the collision energy and H_2(v) state.

A complication of the QCT method is the binning of product states into discrete quantum state energy levels. If classical products are near the energetic limit, the assigned quantum state may be forbidden by energy conservation. A simple solution would be to ignore these energetically forbidden states. We decided instead to include in an approximate way some of the

QCT information in the fitting procedure. This was done by replacing a discrete quantum energy level by a distribution of discrete energies that span the classical energy bin for that level up to the energetic limit. (This yields OH fractional internal energies which can be slightly larger than 1.0, as seen in Figure 7.) Priors were calculated by summing over this discrete distribution. The results turned out to be insensitive to the number of discrete points in the distribution so long as they spanned the energy bin. This procedure made a modest change in the fitted parameters compared to completely ignoring the energetically forbidden quantum states.

C.2. OH (v',j') state distributions

The information theory expression for the OH vibration-rotation state distribution is[16,17]

$$P_{v'j'} = P_0(v',j') (2j'+1) \exp(-S(v',j')). \quad (4)$$

Here $P_0 \sim (E_{trans})^{1/2} = (E - E(v',j'))^{1/2}$ is the density of states for free translation, where E_{trans} is the product translational energy, expressed in terms of the total product energy E and the OH internal energy E(v',j'). The surprisal S(v',j') can be factored into vibrational and rotational parts, $S_{v'}$ and $S_{j'}$, which are functions of vibrational energy $E_{v'}$ and rotational energy $E_{j'}$, respectively. The rotational surprisal, $-\ln(P_{v'j'}/P_0(v',j'))$ at fixed v', may contain v'-dependent parameters. Information theory suggests that the rotational surprisal is likely to be linear in $E_{j'}$ and to approach constancy (statistical behavior) at high energy.

Figure 9 shows plots of the rotational surprisal versus G_r, the fractional available OH rotational energy, $(E_{j'}/(E-E_{v'}))$, at E_{coll} = 10 kcal/mol and 26 kcal/mol for H_2 v=1 and 3. Like the vibrational surprisals, many of these plots are also non-linear. However, the non-linearity, which is most pronounced when high rotational states are populated, is a smooth upward curvature rather than a "V" shape characteristic of an energy-gap law. This behavior is consistent with an angular momentum constraint, which is not accounted for in the conventional information theory prior distribution. We note that for these plots the normalization is such that the $P_{v'j'}$ summed over v' and j' is unity.

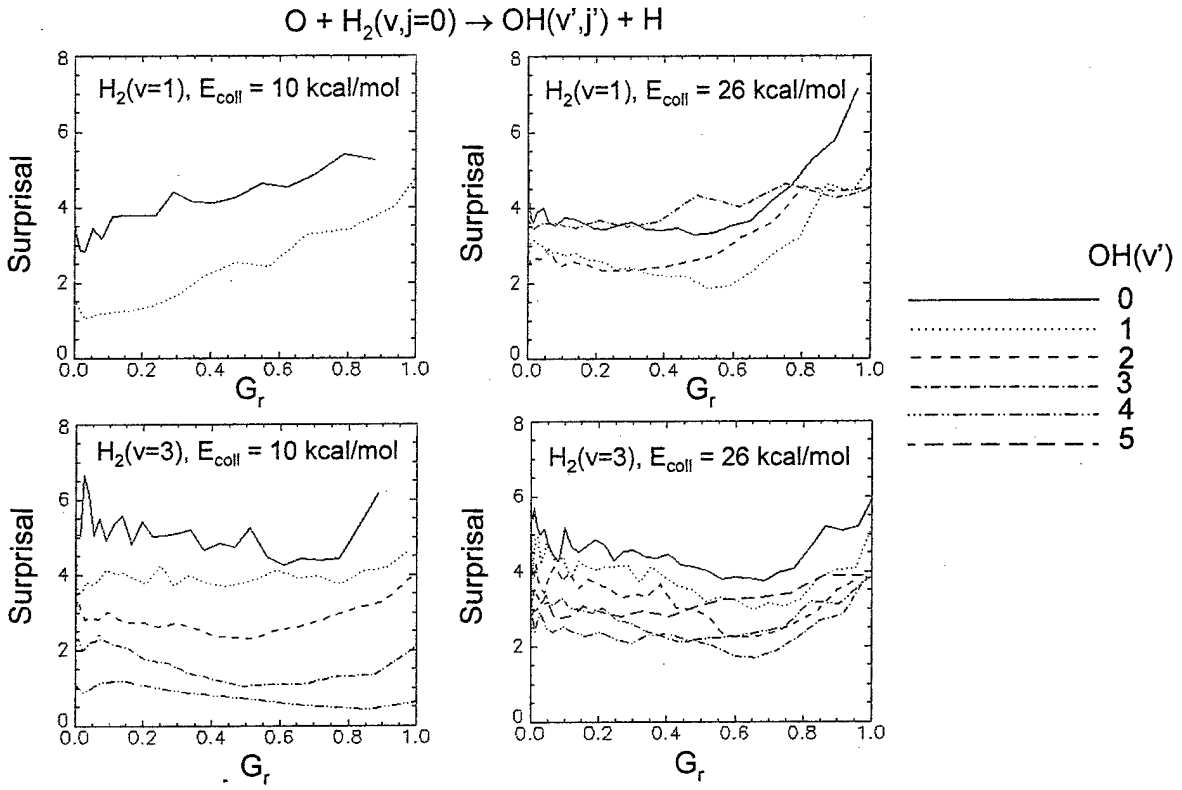

FIG. 9. OH rotational surprisals for $H_2(v)=1$ and 3 using conventional information theory prior distributions. The abscissa is $G_r = (E_{j'}/(E-E_{v'}))$. Results are given at E_{coll} = 10 and 26 kcal/mol for all available OH(v') states.

A statistical dynamics approach that incorporates angular momentum constraints is the PS/OTS (phase space/orbiting transition state) model.[19] In this model, which has been used quite successfully to explain product rotational distributions from chemical reactions and unimolecular decomposition, the precursor to the products is an orbiting collision complex that adiabatically converts its rotational ("orbital") energy into product translation. The statistical product distribution is derived from a direct count of quantum states of the complex subject to conservation of angular momentum. The product high-j' populations are constrained because their high angular momentum must be balanced by a correspondingly high orbital angular momentum, which is limited by the size of the complex, defined by the maximum impact parameter for the reverse reaction. We also note the importance of the H + OH product mass combination in the present case that will limit the amount of final orbital angular momentum.

The PS/OTS calculations are somewhat complicated and not very convenient for empirical fitting. As an alternative, we propose an approximate, analytical prior distribution, $P_0^{\#}$, which is derived by applying analogous angular momentum and impact parameter restrictions to the product translational density of states (see the Appendix). As shown in Figure 10, this modified distribution, which contains two adjustable parameters, leads to surprisal plots that are more linear than those obtained with the standard information theory P_0, making it easier to parameterize the QCT results. Except for a few j' states near the energetic limit, the surprisal plots are essentially flat for $H_2(v=3)$, indicating statistical population of the rotational states within the context of this prior distribution. We note that priors incorporating angular momentum constraints have been used before, and they have been shown to greatly affect the internal state distributions.[26,27]

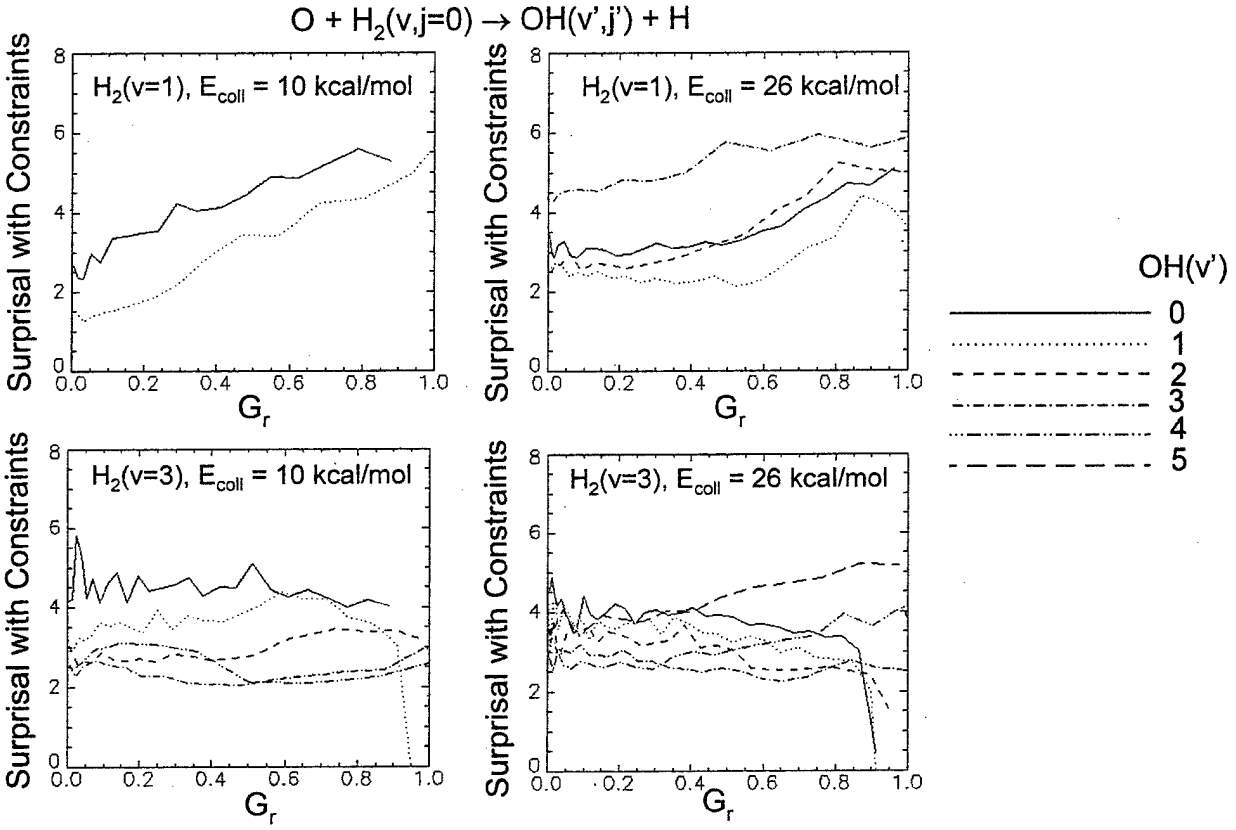

FIG. 10. As in Figure 9, but using the modified prior distributions with angular momentum constraints as discussed in the text.

IV. SUMMARY

We have presented results of time dependent quantum mechanics (TDQM) and quasi-classical trajectory (QCT) studies of the excitation functions for $O(^3P) + H_2(v=0\text{-}3,j=0) \rightarrow OH + H$, on benchmark potential energy surfaces from threshold to 30 kcal/mol. For $H_2(v=0)$ there is excellent agreement between quantum and classical results. The TDQM results show a relatively large (4 kcal/mol) lowering of the threshold energy in going from v=0 to v=1, and then a much smaller lowering (about 1 kcal/mol) in going from v=1 to v=2 and from v=2 to v=3. This suggests that the effective bottleneck for reaction moves up rapidly in energy in going from v=0 to v=1, but not for higher v. In addition, this reaction provides an example where even though the reagent energy is well above the saddle point energy, the reaction is still activated.

For $H_2(v>0)$, the classical results are larger than the quantum results by a factor ~2 near threshold, but the agreement monotonically improves until they are within ~10% near 30 kcal/mol collision energy. We believe this is due to stronger vibrational adiabaticity in the TDQM results. QCT OH(v',j') state-resolved cross sections and angular distributions have also been computed. The QCT vibrationally resolved OH(v') cross sections peak at the same vibrational quantum number as the H_2 reagent. The OH rotational distributions are also quite 'hot' and tend to cluster around high rotational quantum numbers. The state-resolved OH distributions were fit to probability functions based on conventional information theory extended to include an 'energy gap' law for product vibrations and additional angular momentum constraints for product rotations. The fits were generally very good for vibration, and the modified surprisals for rotation were generally linear as a function of collision energy for all transitions.

ACKNOWLEDGEMENTS

M. B. and S. A.-G. acknowledge support through a small business innovative research (SBIR) grant from the Missile Defense Agency (MDA) Contract No. F04611-03-C-0015. M. B. and S. A.-G. thank Lt. M. Morello and Dr. M. Venner of the Air Force Research Laboratory for technical oversight of this work. M. B. and S. A-G. also acknowledge several helpful technical discussions with Drs. L. Bernstein, R. Shroll, J. A. Cline, and J. Duff who provided the quasi-

classical trajectory code used in this work. Thanks are also due to Professor A. Kuppermann and Dr. D. Wang for providing the computer program for the potential surfaces used in this work and to Professor T. Minton for providing the original experimental data for the O + H_2 excitation function.

B. M. and G. C. S. acknowledge the Air Force Office of Scientific Research MURI Center for Materials Chemistry in the Space Environment (AFOSR-F49620-01-1-0335), and the National Science Foundation (CHE-0131998).

Appendix: Derivation of the modified prior distribution for OH v',j' states

We write the prior distribution as the product of the rotational and translational density of states, $\rho_{trans}\,\rho_{rot}$. However, we include only those states satisfying conservation of angular momentum. The translational states included are those whose reverse reaction impact parameter, b, corresponds to an allowed range of translational angular momentum $L_t = \mu b v_{rel}$, μ being the reduced mass of the products and v_{rel} their relative velocity. At fixed v_{rel} the density of three-dimensional translational states is proportional to v_{rel} and the spatial volume they occupy. In our model the volume is a cylinder with diameter b_r, the maximum impact parameter for the reverse reaction, oriented along the translation direction. Without any angular momentum restriction, the phase space volume is proportional to the cross-sectional area of the cylinder, $\frac{1}{4}\pi b_r^2$. With angular momentum restricted to between L_{min} and L_{max}, the volume is proportional to the annular area $\frac{1}{4}\pi(b_{max}^2 - b_{min}^2)$ bounded by $b_{max} = L_{max}/\mu v_{rel}$ and $b_{min} = L_{min}/\mu v_{rel}$, where $b_{min} \le b_{max} \le b_r$. Therefore,

$$P_0^{\#} \sim \rho_{rot}\, v_{rel}(b_{max}^2 - b_{min}^2). \qquad \text{(A1)}$$

By angular momentum conservation, the vector sum of the collisional and reagent angular momenta equals the vector sum of the product translational and rotational angular momenta. Therefore, the translational angular momentum limits are given by

$$L_{max} = \text{the smaller of } L_{coll} + L_i + L_p \text{ and } \mu b_r v_{rel} \qquad \text{(A2a)}$$

$$L_{min} = \text{the smaller of } \big|\,|L_{coll} + L_i| - L_p\,\big| \text{ and } \big|\,|L_{coll} - L_i| - L_p\,\big|. \qquad \text{(A2b)}$$

Here L_{coll} is the angular momentum associated with the collision (forward reaction) impact parameter and velocity, L_i is the angular momentum of the H_2 reagent and L_p is the angular

momentum of the OH product. In the present study $L_i = 0$. $P_0^{\#}$ may be calculated by integrating over the collision impact parameter from 0 to its maximum value. Alternatively, a single impact parameter close to the RMS gives similar results.

Specifying the magnitudes of L_{coll}, L_p and L_t uniquely specifies the direction of the OH angular momentum vector. Therefore, only a specific m_j component of the j manifold should be counted in the rotational density of states. As a result, ρ_{rot} must contain the factor $1/(2j'+1)$, which cancels the $2j'+1$ factor appearing in Equation (4).

Equation (A1) depends on the collision energy, product translational energy, and OH rotational energy as well as on the forward and reverse reaction maximum impact parameters. For long-range R^{-6} potentials, the maximum impact parameter scales as $E_{trans}^{-1/6}$ (see Ref. 18). Combining constants and setting $L_i = 0$ leads to the simple functional form

$$P_0^{\#} \sim E_{trans}^{1/6}(f_{max} - f_{min})/(2j'+1) \tag{A3}$$

where

$$f_{max} = \text{the smaller of 1 and } (k_1 E_{coll}^{1/3} + k_2 E_j^{1/2})^2/E_{trans}^{2/3} \tag{A4a}$$

$$f_{min} = \text{the smaller of 1 and } (k_1 E_{coll}^{1/3} - k_2 E_j^{1/2})^2/E_{trans}^{2/3}. \tag{A4b}$$

In Eq. (A4), k_1 and k_2, which are related to the maximum impact parameters, are taken as empirical fitting parameters. By trial and error we have found suitable values for the H_2 + O reaction to be $k_1 = 0.2$ and $k_2 = 0.17$ kcal/mol$^{-1/6}$. Similar $P_0^{\#}$ results are obtained with forward impact parameter integration, in which a weighted averaging of Eq. (A3) is performed over the k_1=0 to 0.3 range.

REFERENCES

1. D. J. Garton, T. Minton, B. Maiti, D. Troya, and G. C. Schatz, *J. Chem. Phys.* **118**, 1585 (2003).

2. S. Rogers, D. Wang, A. Kuppermann, and S. Walch, *J. Phys. Chem. A* **104**, 2308 (2000).

3. N. Balakrishnan, *J. Chem. Phys.* **119**, 195 (2003).

4. D. Chatfield, R. S. Friedman, G. Lynch, and D. G. Truhlar, *J. Chem. Phys.* **98**, 342 (1993).

5. G. C. Schatz, *J. Chem. Phys.* **83**, 5677 (1985).

6. J.-B. Song and E. A. Gislason, *J. Chem. Phys.* **105**, 10429 (1996).

7. J. M. Bowman, A. F. Wagner, S. P. Walch, and T. H. Dunning Jr., *J. Chem. Phys.* **81**, 1739 (1984).

8. K. T. Lee, J. M. Bowman, A. F. Wagner, and G. C. Schatz, *J. Chem. Phys.* **76**, 3563 (1982).

9. K. T. Lee, J. M. Bowman, A. F. Wagner, and G. C. Schatz, *J. Chem. Phys.* **76**, 3583 (1982).

10. M. Broida and A. Persky, *J. Chem. Phys.* **80**, 3687 (1984).

11. B. R. Johnson and N. W. Winter, *J. Chem. Phys.* **66**, 4116 (1977).

12. R. Schinke and W. A. Lester, *J. Chem. Phys.* **70**, 4893 (1979).

13. N. Cohen and K. R. Westberg, *J. Phys. Chem. Ref. Data* **12**, 554 (1983).

14. P. W. Barnes, I. R. Simes, I. W. M. Smith, G. Lendvay, and G. C. Schatz, *J. Chem. Phys.* **115**, 4586 (2001).

15. G. C. Light, *J. Chem. Phys.* **68**, 2831 (1978).

16. R. D. Levine and R. B. Bernstein, "Molecular Reaction Dynamics and Chemical Reactivity", chapter 5, Oxford University Press, (1987).

17. R. D. Levine and J. Manz, *J. Chem. Phys.* **63**, 4280 (1975).

18. I. Procaccia and R. D. Levine, *J. Chem. Phys.* **63**, 4261 (1975).

19. P. Pechukas and J. C. Light, *J. Chem. Phys.* **42**, 3281 (1965).

20. J. C. Light and J. Lin, *J. Chem. Phys.* **32**, 3209 (1965).

21. G. E. Caledonia, "Infrared Radiation Produced in Ambient/Spacecraft-Emitted Gas Interactions Under LEO Conditions", AIAA 00-0104, 38th AIAA Aerospace Sciences Meeting and Exhibit, 10-13 January 2000, Reno, Nevada.

22. B. Maiti, C. Kalyanaraman, A. N. Panda, And N. Sathyamurthy, J. *Chem. Phys.* **117**, 9719 (2002).

23. D. G. Truhlar and J. T. Muckerman, "Reactive Scattering Cross Sections III: Quasiclassical and Semiclassical Methods", in Atom-Molecular Collision Theory edited by R. B. Bernstein, Plenum Press, New York, 1979.

24. G. C. Schatz, *J. Chem. Phys.* **79**, 5386 (1983).

25. K. P. Huber and G. Herzberg, "Molecular Spectra and Molecular Structure IV. Constants of Diatomic Molecules", Van Nostrand Reinhold Company, New York, 1979.

26. M. S. Fitzcharles and G. Schatz, *J. Phys. Chem.* **90**, 3634 (1986).

27. P. Pechukas, J. C. Light, and C. Rankin, *J. Chem. Phys.* **44**, 794 (1966).